Antarct. Meteorite Res., **10**, 13–40, 1997

PETROLOGY AND MINERALOGY OF THE Y-793605 MARTIAN METEORITE

Yukio IKEDA

Department of Earth Sciences, Ibaraki University, Mito 310

Abstract: Yamato-793605 is a lherzolitic shergottite and very similar in texture and mineralogy to other two lherzolitic shergottites, ALHA77005 and LEW88516, but is not a pair with the latter two. It consists mainly of olivine, pyroxene, maskelynite, chromite, ilmenite, and pyrrhotite. Small silicate inclusions occur in olivine and pyroxene. Olivine has a wide compositional range from Fo_{25} to Fo_{36}, that included in pyroxene is more magnesian, and that in contact with maskelynite is more ferroan. Chromite shows remarkable compositional zoning, and the ranges change according to the occurrence of chromite; chromite included in olivine is Cr-Ti-poor, that in pyroxene is Cr-rich and Ti-poor, and that in contact with maskelynite is Ti-rich. There is a compositional gap between chromites in olivine and pyroxene. Silicate inclusions in olivine consist mainly of aluminous pyroxene, fine-grained intergrowth of plagioclase and silica, and rhyolitic glass. Plagioclase of the intergrowth is more calcic with An_{63-83} than maskelynite of the host lithology (An_{30-58}). The rhyolitic glass saturates with silica components and is peraluminous, whereas the host lithology does not include any silica mineral and is not peraluminous. These differences between the silicate inclusions and the host lithology, as well as the compositional gap between chromites in olivine and pyroxene, suggest that magma mixing took place in the Y-793605 magma reservoir between olivine and pyroxene crystallization stages. Y-793605 experienced secondary alteration of olivine, non-rhyolitic glass, chromite, ilmenite, pyrrhotite, and phosphate by introduction of Si and K, and loss of Ti, Cr, Mg, Ca, and Na probably at Antarctica.

1. Introduction

Martian meteorites include seven shergottites, three nakhlites, one chassignite, and one martian orthopyroxenite (or martian diogenite). They all are igneous rocks, and the study of them is revealing the nature of martian igneous activity (MCSWEEN, 1994). Yamato-793605 is one of shergottites, has a lherzolitic mineral assemblage, and is very similar in mineralogy and texture to ALHA77005 and LEW88516 (MIKOUCHI and MIYAMOTO, 1996).

Y-793605 is studied by the Y-793605 research consortium (leaders: H. KOJIMA, P. WARREN, M. MIYAMOTO, and K. YANAI organized by NIPR), and this paper covers the petrology and mineralogy of Y-793605 as one of the consortium study.

2. Analytical Methods

Minerals and glass in Y-793605 were analysed using an electron-probe micro-analyser (EPMA, JEOL superprobe 733) with beam current of 3–6 nA, accelerating

voltage of 15 kV, and counting time of 10 s. The correction method of BENCE and ALBEE (1968) was employed for silicates and oxides, and the standard ZAF method for sulfides.

In order to prevent the evaporation loss of alkalies during the EPMA analyses, 3 nA of beam current and 10 s of counting time were used for maskelynite and glass in silicate inclusions. However, alkali loss seems to still happen during the EPMS analyses of the glassy materials with a focussed beam. To check the degrees of the alkali loss, I compared the Na_2O and K_2O contents of the same glassy materials obtained by a focussed beam with those obtained by a defocussed beam with a 10 μm diameter under the same conditions; the contents obtained by the latter were higher by a factor of 1.05 on average than those by the former. In spite of the result, the analyses using a focussed beam was employed in this paper, because glass in silicate inclusions in Y-793605 is often very small. The Na_2O and K_2O contents obtained by the focussed-beam analyses were multiplied by a factor of 1.05 for maskelynite and glass in silicate inclsuions.

3. Petrography

3.1. Sample description

Y-793605 includes two different lithologies: poikilitic and non-poikilitic, which are very similar to those of ALHA77005 and LEW88516 (MIKOUCHI and MIYAMOTO, 1996). Two thin sections of Y-793605 (50-1, 51-1) were used for this study, and their overall textures are shown in KOJIMA *et al.* (1997); one thin section (50-1) shows almost a poikilitic texture with chadacrystic olivine and oikocrystic pyroxene, and the other thin section (51-1) shows a layer of non-poikilitic lithology intercalated in between two layers of poikilitic lithology. The mineral compositions of the poikilitic and non-poikilitic portions are similar to each other, but olivine and pyroxene are slightly more ferroan in the latter than in the former (MIKOUCHI and MIYAMOTO, 1996).

The constituent minerals of the Y-793605 lithologies are olivine, pigeonite, augite, maskelynite, non-rhyolitic glass, chromite, ilmenite, baddeleyite, and sulfide. Olivine and opaque minerals such as chromite, ilmenite, and sulfide have locally experienced weathering alteration. Small silicate inclusions occur in chadacrystic olivine and oikocrystic pyroxene grains.

The modal compositions of Y-793605 are shown in Table 1. Pyroxene is more abundant than olivine in one thin section (50-1), whereas olivine is more in the other thin section (51-1). This results from the fact that the former thin section (50-1) is predominantly poikilitic lithology which includes oikocrystic pyroxene more abundantly than chadacrystic olivine. The normative composition of Y-793605, which was calculated from the bulk composition obtained by WARREN and KALLEMEYN (1997), is between the modal compositions of the two thin sections and similar to the average compostion (Table 1).

3.2. Silicate inclusions

3.2.1. Silicate inclusions in chadacrystic olivine grains

Silicate inclusions with rounded or ellipsoidal outlines are often included in

Table 1. Modal composition (vol %) of Y-793605. Two thin sections (subnumbers, 50-1 and 51-1) are used for the modal analyses. The area ratio of the two thin sections, 50-1 and 51-1, is 43.3% and 56.7% respectively and the average is obtained by multiplying the ratio. The normative composition calculated from the bulk composition (WARREN and KALLEMEYN, 1997) is shown for reference: the norm is given here in mole%, and all the moleculars are set for O=24 which may represent their volumes in zero approximation.

Thin section	50-1	51-1	Average	Normative composition
Olivine	28.4	49.5	40.4	44.3 [(Mg, Fe)$_{12}$Si$_6$O$_{24}$]
Pyroxene	68.5	37.3	50.8	45.4 [(Ca, Mg, Fe)$_8$Si$_8$O$_{24}$]
Maskelynite	2.1	11.5	7.4	8.8 [Ca$_3$Si$_6$Al$_6$O$_{24}$ + (Na, K)$_3$Si$_9$Al$_3$O$_{24}$]
Opaque minerals	1.0	1.7	1.4	1.5
Chromite	0.95	1.29	1.2	1.0 [Fe$_6$Cr$_{12}$O$_{24}$]
Ilmenite	0.04	0.34	0.2	0.5 [Fe$_8$Ti$_8$O$_{24}$]
Sulfide	0.01	0.07	0.04	

Methods of modal analyses: a sheet of transparent paper with sections was covered on enlarged back-scattered-electron images of each thin section, outlines of each mineral grain were drown on the sheet, and the areas were counted for each mineral.

chadacrystic olivine grains (Fig. 1l, m, n, o). Their size ranges from 10 to 150 μm across. They consist mainly of rhyolitic glass, fine-grained intergrowth of plagioclase and silica, and/or aluminous pyroxene with or without silica-predominant glass, plagioclase, Al-rich spinel, ilmenite, and sulfide. The modal amounts of the rhyolitic glass and the intergrowth are various among silicate inclusions, but they seem to nearly equal to each other as a whole. All plagioclases in silicate inclusions seem to be isotropic under an optical microscope, suggesting that an impact shock changed the plagioclase to maskelynite. In this paper the term "plagioclase" is used for the maskelynite in silicate inclusions because of its distinction from the maskelynite in the host lithology. Pyroxenes in silicate inclusions are euhedral (Fig. 1l, m, n, o) and sometimes grow from the inclusion walls (Fig. 1l, m, o). Silica-predominant glass has rounded or ovoidal outlines, a few to a few tens of μm in diameter. It is often included by the fine-grained intergrowth of plagioclase and silica in silicate inclusions.

3.2.2. Silicate inclusions in oikocrystic pyroxene grains

Oikocrystic pyroxene also includes small silicate inclusions with irregular outline (Fig. 1p, q, r). They are 10 to a few tens of μm in width and up to 100 μm in length. They sometimes show rectanglar outlines which elongate parallel to the *c*-axis of the oikocrystic pyroxene. They consist mainly of rhyolitic glass and minor pyroxene crystals with or without plagioclase, ilmenite and spinel (Fig. 1p, q).

3.3. Impact shock effects

Chadacrystic olivine in Y-793605 often shows mozaic extinction under an optical microscope with corssed Nicols (Fig. 1a). In addition, many weak fractures are pervasive throughout olivine grains (Fig. 1a). These features may be due to impact shock events. Oikocrystic pyroxene also has many weak fractures (Fig. 1c) similar to those in olivine, but the degree of fracturing for pyroxene seems to be less than that for olivine. Microscopic observation reveals that some planar fractures, which cut

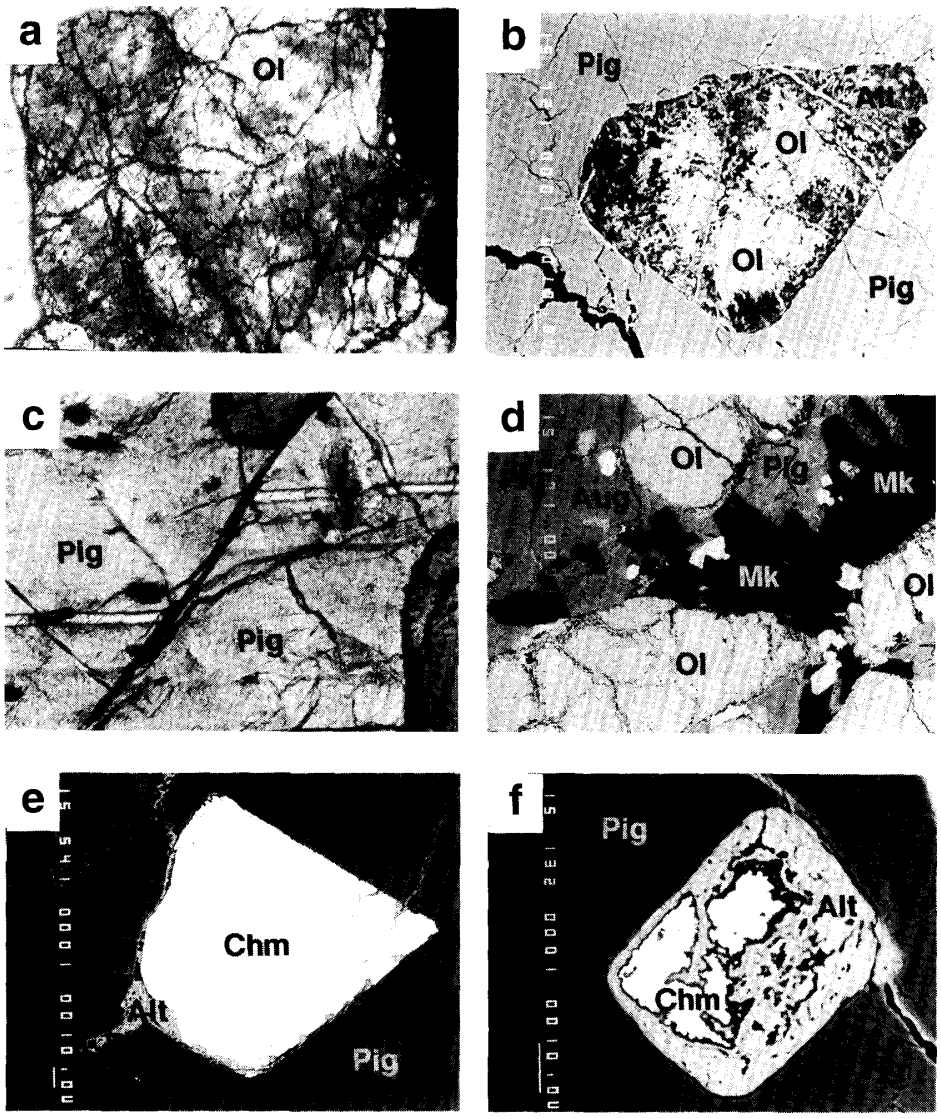

Fig. 1. Optical photomicrographs and back-scattered-electron (BSE) images of Y-793605.

a. Photomicrograph (crossed Nicols) of a chadacrystic olivine (Ol) grain. Note the mozaic extinction of olivine and small fractures throughout the grain. Secondary alteration products occur along network fractures which are wider and more clear than the small fractures. Width is 1 mm.

b. BSE image of a chadacrystic olivine grain included in oikocrystic pigeonite (Pig). Note that secondary alteration products (Alt) occur along the rim and fractures. Width is 160 μm.

c. Photomicrograph (crossed Nicols) of oikocrystic pigeonite. Note that a twin in pigeonite displaces along a straight fracture in a distance of about 200 μm. Width is 500 μm.

d. BSE image of maskelynite (Mk), augite (Aug), pigeonite (Pig) and olivine (Ol). Note that maskelynite occurs interstitially between olivine and pyroxene. Augite occurs in close association with maskelynite. Width is 1.2 mm.

e. BSE image of chromite (Chm) in pigeonite. Note that chromite altered by weathering along the rim. Width is 210 μm.

f. BSE image of chromite in pigeonite. Most of this chromite altered by weathering. Width is 90 μm.

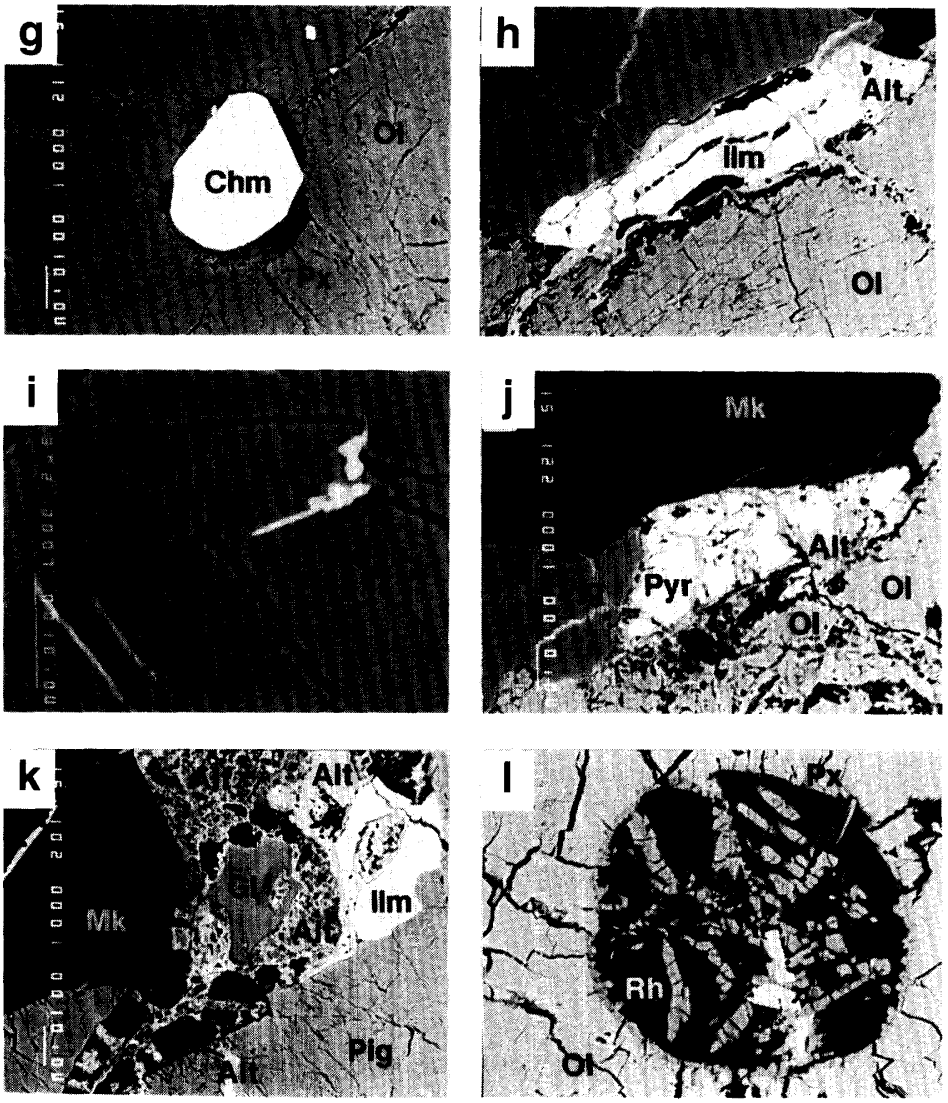

Fig. 1 (Continued).

g. BSE image of chromite in chadacrystic olivine. Note that chromite occurs in close association with aluminous pyroxene (Px). Width is 100 μm.

h. BSE image of ilmenite (Ilm). Note that ilmenite occurs near or in contact with maskelynite (upper right, black) and that secondary alteration products (Alt) occur along the rim and fractures in ilmenite. Width is 140 μm.

i. BSE image of baddeleyite (Bd) occurring in ilmenite (Ilm). Width is 40 μm.

j. BSE image of pyrrhotite (Pyr). Note that pyrrhotite altered along the rim and fractures. Width is 100 μm.

k. BSE image of non-rhyolitic glass (Gl). It occurs in weathering alteration zone between maskelynite (Mk), ilmenite (Ilm), and pigeonite (Pig). Dark phase (Alt) with an arrow is Si-Al-Fe-rich alteration products, and alteration products near ilmenite (upper right, gray) is Fe-K-S type. Width is 120 μm.

l. BSE image of a magmatic silicate inclusion in chadacrystic olivine. Rhyolitic glass (Rh) occurs in contact with fine-grained intergrowth of plagioclase and silica (PS). Aluminous pyroxene needles (Px) and opaque minerals (Cr-rich spinel, ilmenite, and sulfide; white) set in both rhyolitic glass and the fine-grained intergrowth. Width is 100 μm.

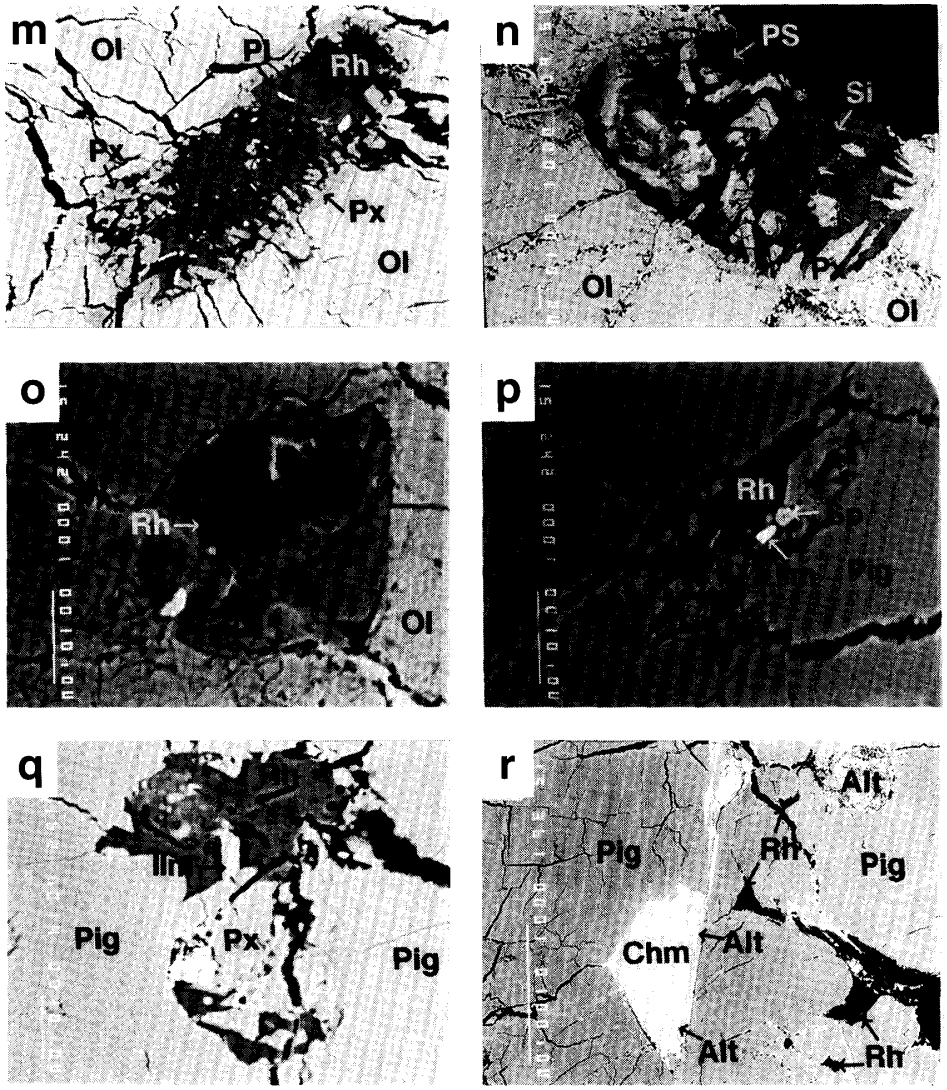

Fig. 1 (Continued).

m. BSE image of a magmatic silicate inclusion in chadacrystic olivine. Fine-grained intergrowth of plagioclase and silica (PS) occurs in the central portion, and plagioclase grains (Pl; they are now maskelynite) grow at the rims, protruding into rhyolitic glass (Rh). Aluminous pyroxene (Px) occurs lining the inclusion wall and as small euhedral grains in the rhyolitic glass and the PS intergrowth. Width is 120 μm.

n. BSE image of a magmatic silicate inclusion in chadacrystic olivine. Note that fine-grained intergrowth of plagioclase and silica (PS, gray) includes silica-predominant glass (Si, dark) with subrounded or ovoidal shapes. Aluminous pyroxene (Px) occurs lining the inclusion wall and as euhedral grains in the inclusion. Width is 190 μm.

o. BSE image of a magmatic silicate inclusion in chadacrystic olivine. Rhyolitic glass (Rh) occurs in interstitial spaces between aluminous pyroxene grains (Px). A small chromite grain (lower left within the inclusion, white) sets in pyroxene. Width is 50 μm.

p. BSE image of a silicate inclusion in oikocrystic pyroxene (Pig). Note that this inclusion has an irregular outline and consists of rhyolitic glass (Rh), aluminous pyroxene (Px), ilmenite (Ilm), and aluminous spinel (Sp). Width is 50 μm.

q. BSE image of a silicate inclusion in oikocrystic pyroxene (Pig). Pyroxene (Px) and ilmenite (Ilm) grains occur in rhyolitic glass (Rh). Width is 73 μm.

r. BSE image of irregularly-shaped rhyolitic glass (Rh) in oikocrystic pyroxene (Pig). A chromite grain in pigeonite was cut and displaced by a straight fracture (center), and the displacement along the fracture is about 100 μm. Note that secondary alteration products (Alt with an arrow) surround the whole chromite grain which was cut by the fracture. Width is 330 μm.

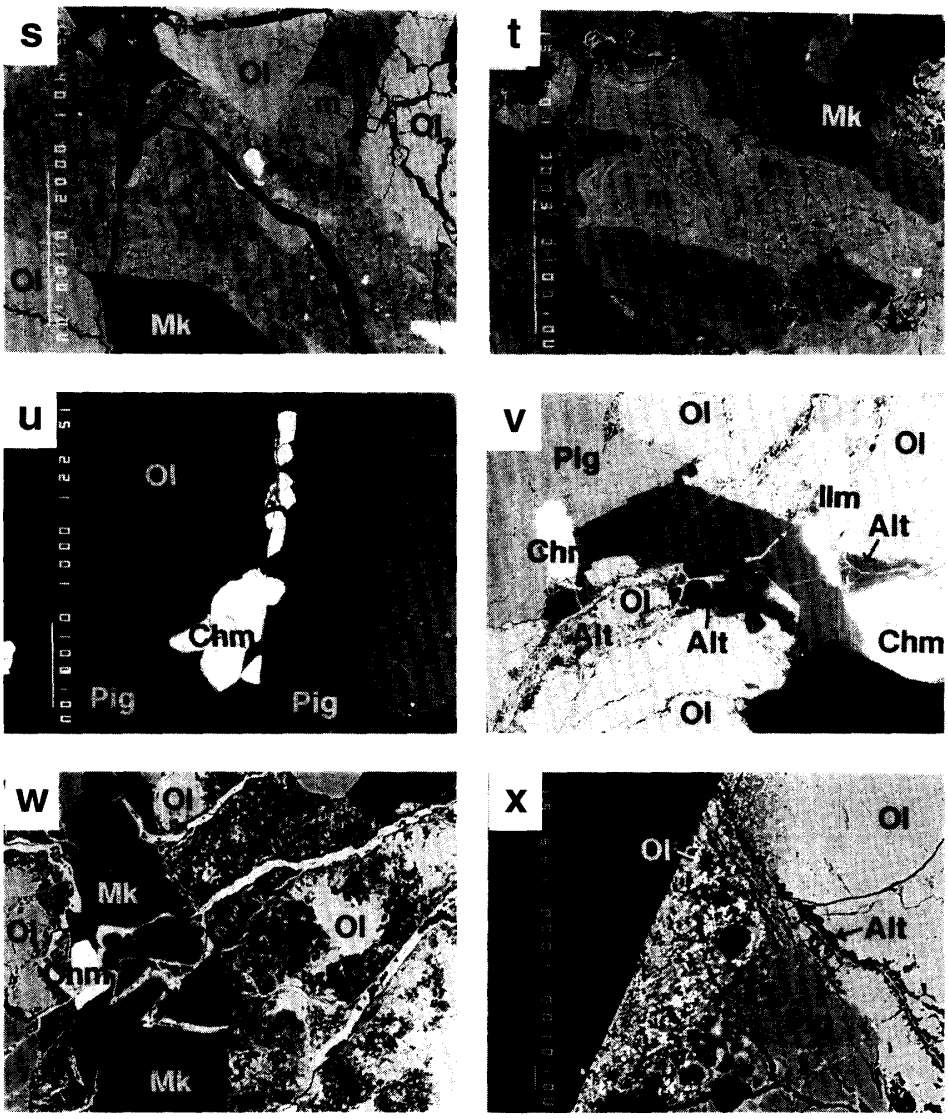

Fig. 1 (Continued).

s. BSE image of a shock-induced crushed zone. Fragmental grains of olivine (Ol with arrows) and chromite (Chm with an arrow) occur in the crushed zone. Glassy substance (m) is found in contact with pigeonitic pyroxene (Pig). Width is 300 μm.

t. BSE image of glassy substance (m) with a "flow" texture. It occurs at an end of a shock-induced crushed zone. Width is 300 μm.

u. BSE image of chromite grains which were cut by a straight fracture (center). Displacement is about 100 μm. Width is 530 μm.

v. BSE image of Si-Al-Fe type alteration products (Alt with an arrow) in contanct with maskelynite (Mk) and olivine (Ol). Width is 600 μm.

w. BSE image of alteration products of Si-Fe-Mg type (right half of the figure) around relic olivine grains (Ol). Note that weathering veinlets (white) cut a maskelynite (Mk) grain and Si-Fe-Mg type alteration products. Width is 170 μm.

x. BSE image of a fusion crust of Y-793505. Magnesian olivine (Ol with an arrow, dark) occurs in close association with tiny grains (white) of an Fe-phase (probably magnetite or hematite). Alteration products occurs as veinlets in olivine (Ol) and seem to cut the fusion crust. Width is 170 μm.

oikocrystic pyroxene grains, dispaced the oikocrystic pyroxene and chromite grains in distance up to 200 μm (Fig. 1c, r, u). Maskelynite is the main mineral in the non-poikilitic lithology of Y-793605 and was produced from plagioclase by an impact shock event which had probably splashed out Y-793605 from Mars.

A shock-induced crushed zone (Fig. 1s, t) is found in one thin section (51-1) studied. It consists mainly of fine-grained aggregates of crushed minerals, including larger fragments of olivine (Fo_{75-65}), chromite, and ilmenite (Fig. 1s). Small grains of magnesian olivine occur in the fine-grained aggregates. Glassy substance (Fig. 1s, t) is found in the crushed zone and has a texture like a "flow" one (Fig. 1t).

3.4. Fusion crust

Fusion crust is observed in one thin section (51-1) studied. It consists mainly of fine-grained aggregates of silicates and Fe oxides (Fig. 1x). Small magnesian olivine and pyroxene grains occur in the fine-grained aggregates. The phases of Fe-oxides in the aggregates are unknown because they are too small, but probably magnetite or hematite.

4. Mineralogy

4.1. Olivine

Olivines in Y-793605 occur as chadacrysts having subheral to corroded outlines in the poikilitic lithology (Fig. 1b) and as euheral to subhedral crystals in the non-poikilitic lithology (Fig. 1d). Their size ranges from about 50 μm up to about 1 mm in diameter. The chemical compositions of olivines range widely from Fa_{25} to Fa_{36} (Table 2, Fig. 2) and change according to its occurrence; olivines included in maghesian pigeonite are more magnesian (Fa_{25-28}), those included in less-magnesian pigeonite are intermediate (mostly Fa_{28-32}), and those in contact with maskelynite are more ferroan (Fa_{31-36}).

Magnesian olivine (Fo_{85-80}, Table 5) occurs in a shock-induced crushed zone, and more magnesian olivine (Fo_{90-95}, Table 5) is found in the fusion crust.

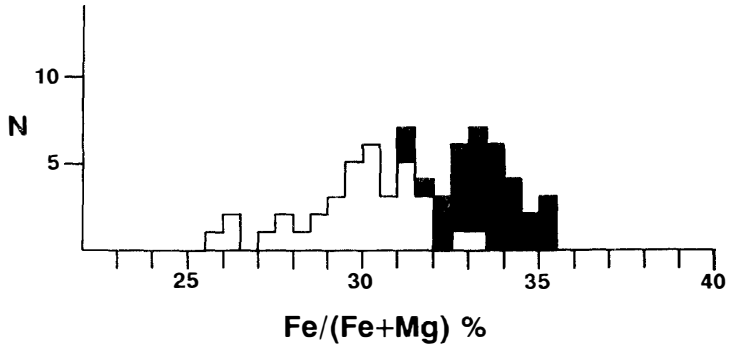

Fig. 2. Histogram of olivine compositions (atomic%). White symbols are chadacrystic olivine included in oikocrystic pyroxene, and black ones are olivine which occurs near or in cantact with maskelynite.

Table 2. Chemical compositions of chadacrystic olivine (Ol), oikocrystic pigeonite (Pig), augite (Aug), non-rhyolitic glass (Gl), maskelynite (Mk), chromite (Chm), and ilmenite (Ilm) in the Yamato-793605.

	1	2	3	4	5	6	7	8
	Ol	Ol	Ol	Pig	Pig	Aug	Gl	Mk
SiO_2	37.33	37.15	36.68	55.19	54.03	51.57	55.25	53.77
TiO_2	0.00	0.00	0.00	0.04	0.00	0.74	1.00	0.01
Al_2O_3	0.00	0.00	0.00	0.31	0.64	1.73	14.83	27.62
Cr_2O_3	0.22	0.00	0.00	0.37	0.46	1.15	0.00	0.00
V_2O_5	—	—	—	—	—	—	—	—
FeO	24.57	27.51	29.67	14.46	16.41	9.84	12.38	0.49
MnO	0.28	0.58	0.54	0.59	0.39	0.27	0.00	0.07
MgO	36.26	33.91	32.37	27.22	23.22	16.78	4.01	0.16
CaO	0.18	0.24	0.21	1.79	4.56	17.17	8.38	11.55
Na_2O	0.00	0.00	0.00	0.00	0.00	0.34	2.59	5.24
K_2O	0.00	0.00	0.00	0.00	0.00	0.00	0.43	0.26
Total	98.83	99.39	99.45	99.96	99.71	99.58	98.89	99.16

	9	10	11	12	13	14	15	16
	Mk	Mk	Chm	Chm	Chm	Chm	Chm	Ilm
SiO_2	53.99	57.39	0.00	0.00	0.00	0.00	0.00	0.00
TiO_2	0.00	0.06	1.40	2.45	1.00	1.11	14.30	53.39
Al_2O_3	27.60	25.83	10.47	13.19	5.81	6.66	5.16	0.00
Cr_2O_3	0.00	0.00	51.00	46.10	58.61	59.12	30.96	0.47
V_2O_5	—	—	0.65	0.55	0.47	—	—	0.13
FeO	0.72	0.24	29.52	31.59	26.58	28.84	43.28	37.97
MnO	0.00	0.00	0.77	0.59	0.71	0.18	0.44	0.59
MgO	0.15	0.09	4.28	3.94	5.89	4.20	3.45	5.39
CaO	10.95	8.95	0.00	0.00	0.00	0.00	0.00	0.00
Na_2O	5.42	5.97	0.00	0.00	0.00	0.00	0.00	0.00
K_2O	0.31	0.50	0.00	0.00	0.00	0.00	0.00	0.00
Total	99.12	99.03	98.10	98.40	99.07	100.12	97.60	97.94

Column 1 is magnesian olivine included in magnesian low-Ca pigeonite such as Column 4. Column 3 is ferroan olivine directly in contact with maskelynite. Magnesian low-Ca pigeonite of Column 4 may have been originally orthopyroxene before impact shock. Columns 11 and 12 are chromite included in chadacrystic olivine, Column 13 is chromite included in oikocrystic pigeonite, and chromite grains of Columns 14 and 15 are directly in contact with maskelynite.

4.2. Pyroxene

Pigeonite occurs as large oikocrysts, up to more than 8 mm in size. The central portions of large pigeonite oikocrysts are more magnesian and poorer in Ca than the mantle and peripheral portions; the magnesian and Ca-poor pigeonite is $En_{73-76}Wo_{2-4}$ (Fig. 3a). Judging from optical microscopic observation it is now clinopyroxene, but it might have been originally orthopyroxene before an intense impact shock changed the orthopyroxene to clinopyroxene. Most pigeonite of the mantle and peripheral portions of the oikocrysts is $En_{63-71}Wo_{7-10}$, although intermediate pyroxene with

$En_{70-73}Wo_{5-7}$ occurs (Fig. 3a). Pigeonite which is just in contact with maskelynite is sometimes subcalcic with $En_{58-64}Wo_{10-17}$. Augite occurs as small grains near or in contact with maskelynite and is $En_{45-50}Wo_{30-40}$ (Fig. 3a). Minor element compositions (Al_2O_3, TiO_2, and Cr_2O_3) of the pyroxenes (Table 2) increase continuously from magnesian and Ca-poor pigeonite to augite via normal pigeonite (Fig. 4).

Pyroxenes in silicate inclusions in chadacrystic olivine grains occur as euhedral crystals sometimes growing from the inclusion walls. They are low-Ca, subcalcic, and fassaitic high-Ca pyroxenes as shown in Fig. 3b. Some of low-Ca pyroxene are poor in Ca, having orthopyroxene compositions of $En_{65-73}Wo_{2-4}$. Pigeonitic pyroxene is $En_{65-70}Wo_{7-10}$. Subcalcic pyroxene changes their compositions continuously from pigeonitic to fassaitic pyroxenes. The fassaitic pyroxene ranges from En_{50} to En_{25} with Wo contents of 37–56 mol% (Fig. 3b). The inclusion pyroxenes are similar in major element compositions to the pyroxenes of the host lithology, but low-Ca pyroxene in silicate inclusions is more ferroan than the oikocrystic pyroxenes (Fig. 3).

The minor element contents of the inclusion pyroxenes in chadacrysts (Table 3) are decidedly different from those of the pyroxenes of the host lithology as shown in Fig. 4; the Al_2O_3 content of the inclusion pyroxenes ranges from 3 wt% to 12 wt%, whereas that of the pyroxenes of the host lithology is lower than 3 wt% (Fig. 4). The TiO_2 content of the inclusion pyroxenes is higher than that of the pyroxenes of the host lithology, but the Cr_2O_3 conent is lower for the inclusion pyroxenes than for the pyroxenes of the host lithology (Fig. 4).

Small euhedral pyroxene grains are rarely found in silicate inclusions in oikocrystic pyroxene grains (Fig. 1p, q). However, most of them are smaller than a few μm across and too small to analyse except for a few cases. There are two types of pyrox-

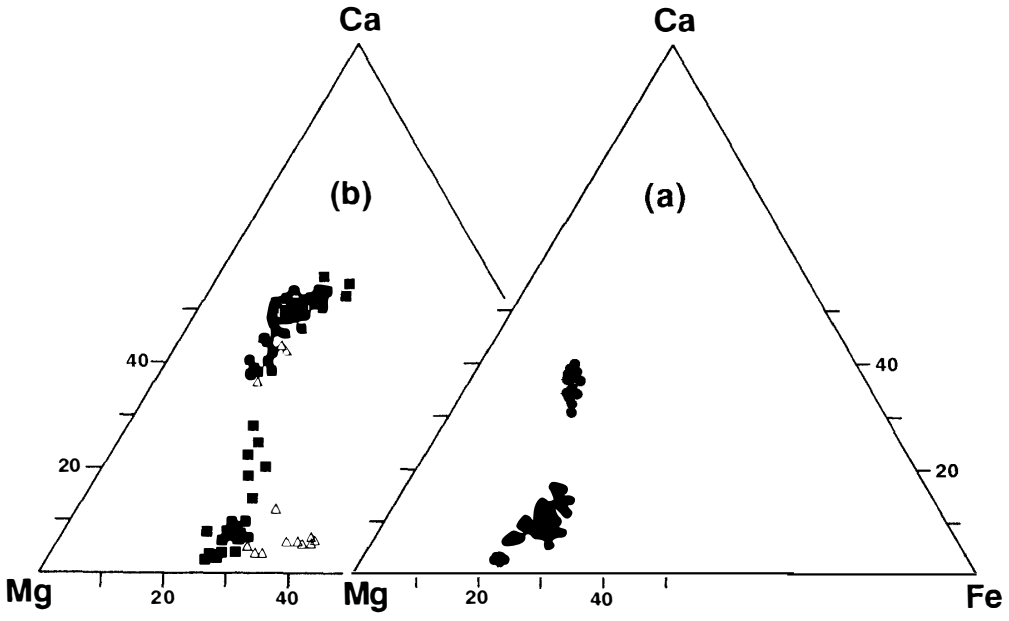

Fig. 3. Ca-Mg-Fe plot (atomic%) of oikocrystic pyroxenes (a) and pyroxenes in silicate inclusions in chadacrystic olivine grains (solid squares, b) and in oikocrystic pyroxene grains (open triangles, b).

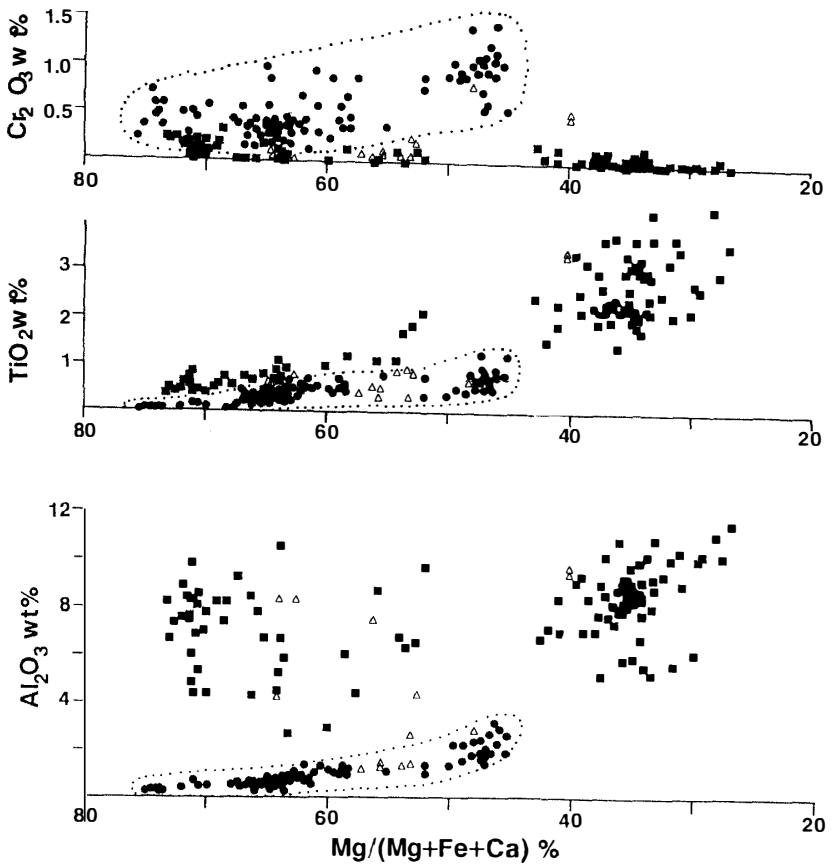

Fig. 4. Minor element compositions (Al_2O_3, TiO_2, and Cr_2O_3) of oikocrystic pyroxenes (solid circles, shown by dotted lines) and pyroxenes in silicate inclusions in chadacrystic olivine grains (solid squares) and in oikocrystic pyroxene grains (open triangles) are plotted against their Mg/(Mg+Fe+Ca) atomic%.

enes in silicate inclusions in oikocrysts, Al-rich and Al-poor pyroxenes. The Al-rich pyroxene is similar in chemical compositions to the aluminous pyroxene in silicate inclusions in chadacrysts (Figs. 3, 4), whereas the Al-poor pyroxene is poor in Al_2O_3 and TiO_2 (Fig. 4) and similar to the oikocrystic pigeonite. However, the Al-poor pyroxene in silicate inclusions is more ferroan than the oikocrystic pigeonite (Fig. 3).

4.3. Maskelynite

Maskelynite occurs in interstitial spaces surrounded by pyroxene and olivine grains. Most of maskelynite have a compositional range from $An_{58}Or_1$ to $An_{50}Or_2$ and often show normal zoning. Sometimes more sodic maskelynite with $An_{30\text{-}50}Or_{1.5\text{-}4.0}$ occurs at the rims of maskelynite grains (Fig. 5).

4.4. Non-rhyolitic glass

A piece of non-rhyolitic glass with an irregular shaped outline, 20 μm in size, occurs in an alteration zone near maskelynite (Fig. 1k). The glass is hogmogeneous and has a non-rhyolitic composition (Table 2). The normative pyroxene composition

Table 3. Chemical compositions of aluminous pyroxene (Px), plagioclase (Pl), fine-grained intergrowth of plagioclase and silica (PS), rhyolitic glass (Gl), and silica-predominant glass (Sil) in silicate inclusions in chadacrystic olivine, and pyroxene (Px), rhyolitic glass (Gl), and spinel (Sp) in silicate inclusions in oikocrystic pyroxene.

	Inclusions in olivine												
	Px	Px	Px	Pl	Pl	PS	PS	Gl	Gl	Gl	Gl	Sil	Sil
SiO_2	49.99	51.11	46.22	46.35	50.89	64.01	65.75	69.59	72.35	69.80	71.85	90.93	93.85
TiO_2	0.53	0.54	2.32	0.00	0.18	0.36	1.02	0.27	0.30	0.20	0.45	0.24	0.22
Al_2O_3	8.11	4.46	8.75	32.98	29.48	20.87	19.91	19.94	17.85	16.57	15.20	5.64	3.65
Cr_2O_3	0.16	0.08	0.00	0.00	0.00	0.00	0.04	0.00	0.00	0.00	0.00	0.01	0.00
FeO	16.56	16.82	8.10	0.73	0.52	0.70	1.73	0.91	1.02	1.19	1.12	0.35	0.00
MnO	0.41	0.51	0.22	0.14	0.11	0.24	0.00	0.00	0.00	0.12	0.08	0.00	0.00
MgO	22.96	22.07	11.62	0.06	0.25	0.36	0.31	0.12	0.16	0.14	0.07	0.07	0.00
CaO	1.48	3.88	21.99	16.29	14.39	10.47	9.21	1.35	1.28	1.35	0.98	1.30	0.24
Na_2O	0.07	0.12	0.12	2.04	3.00	1.75	2.61	6.45	4.20	4.37	4.37	1.63	1.13
K_2O	0.00	0.00	0.03	0.00	0.00	0.00	0.19	0.36	0.59	5.27	4.37	0.21	0.02
P_2O_5	—	—	—	—	—	—	—	—	0.58	—	0.13	—	—
Total	100.25	99.59	99.37	98.59	98.82	98.76	100.77	98.99	98.32	99.01	98.62	100.38	99.12

	Inclusions in pyroxene				
	Px	Px	Gl	Gl	Sp
SiO_2	49.31	44.56	70.89	71.89	0.25
TiO_2	0.93	3.27	0.24	0.30	0.30
Al_2O_3	2.72	9.70	15.99	17.65	57.02
Cr_2O_3	0.25	0.49	0.00	0.00	2.00
FeO	23.59	10.09	0.93	0.71	25.01
MnO	0.77	0.14	0.15	0.00	0.34
MgO	17.64	12.65	0.07	0.19	10.73
CaO	3.21	18.59	1.71	2.35	0.07
Na_2O	0.12	0.42	3.80	5.74	0.06
K_2O	0.00	0.00	5.44	0.59	0.03
P_2O_5	—	0.16	—	—	—
Total	98.53	99.92	99.38	99.42	95.81

Spinel grains in a silicate inclusion are too fine-grained to obtain their good chemical composition.

is $En_{32.2}Fs_{51.6}Wo_{16.2}$, and it has a small amount of normative quartz. The normative feldspar composition is $An_{51.7}Ab_{43.5}Or_{4.8}$ and similar to the composition of maskelynite in the host lithology except its higher Or content.

4.5. Rhyolitic glass in silicate inclusions

Rhyolitic glass is common in silicate inclusions which occur both in chadacrystic olivine and oikocrystic pyroxene grains. It is rhyolitic in chemical compositions (Table 3) and has a wide compositional range as shown in Fig. 6; the composition of rhyolitic glass has a narrow range in one silicate inclusion, but it differs in composition among silicate inclusions even if it occurs in one chadacrystic olivine grain. The

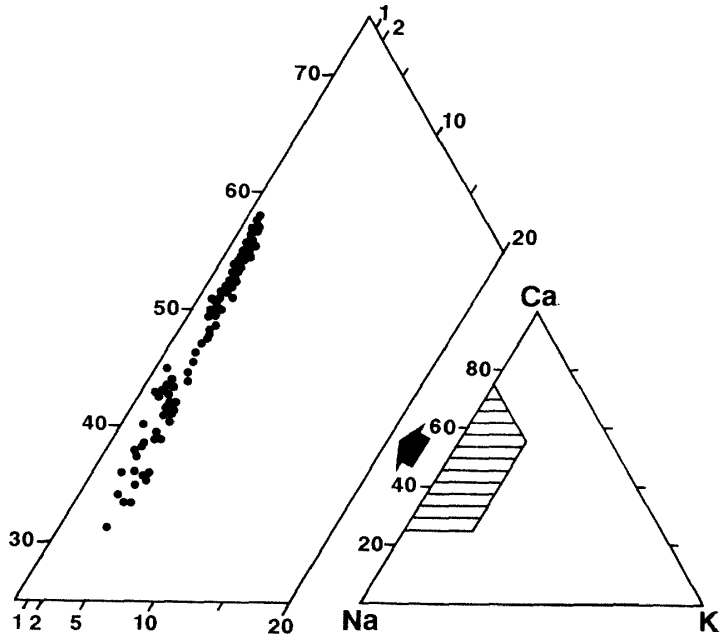

Fig. 5. Ca-Na-K plot (atomic%) of maskelynite in Y-793605. Most of maskelynite concentrate in a range from An_{50} to An_{58}.

K/Na atomic ratios of the glass are always smaller than unity (Fig. 6), but the inclusion glass in oikocrysts seems to be enriched in K_2O as a whole in comparison to the inclusion glass in chadacrysts.

Normative compositions of the rhyolitic glass are plotted in Fig. 7; they distribute both in the feldspar and silica-mineral liquidus fields of the granitic system (Ab-Or-SiO_2-H_2O system, TUTTLE and BOWEN, 1958). The rhyolitic glass in chadacrysts is peraluminous (Table 3, Fig. 8), and often has normative corundum contents, up to 1/3 (wt% ratio) of the normative quartz; the normative corundum contents of Na-rich rhyolitic glass are higher on average than those of K-rich rhyolitic glass in silicate inclusions (Fig. 8).

4.6. Fine-grained intergrowth of plagioclase and silica

Fine-grained intergrowth of plagioclase and silica occurs in close association with the rhyolitic glass in some silicate inclusions in chadacrystic olivine grains (Fig. 1l, m, n). It never occurs in silicate inclsuions in oikocrystic pyroxene grains. The grain size of the intergrowth is various among silicate inclusions, ranging from a few μm to submicroscopic size. Sometimes euhedral plagioclase grains, about 10 μm across, grow at the rims of the intergrowth, protruding into rhyolitic glass (Fig. 1m). The plagioclases are $An_{63\text{-}83}$, and the chemical compositions of the intergrowth are more calcic than the rhyolitic glass above stated (Table 3, Fig. 6a). The intergrowth sometimes contains minor and variable amounts of the rhyolitic glass component (Fig. 6a). Normative compositions of the intergrowth are plotted in Fig. 7; they are poor in the orthoclase component and concentrate in a range from Pl_8Qz_2 to Pl_5Qz_5 where Pl and Qz are normative plagioclase ($CaSi_2Al_2O_8 + NaSi_3AlO_8$) and quartz ($Si_4O_8$) in molec-

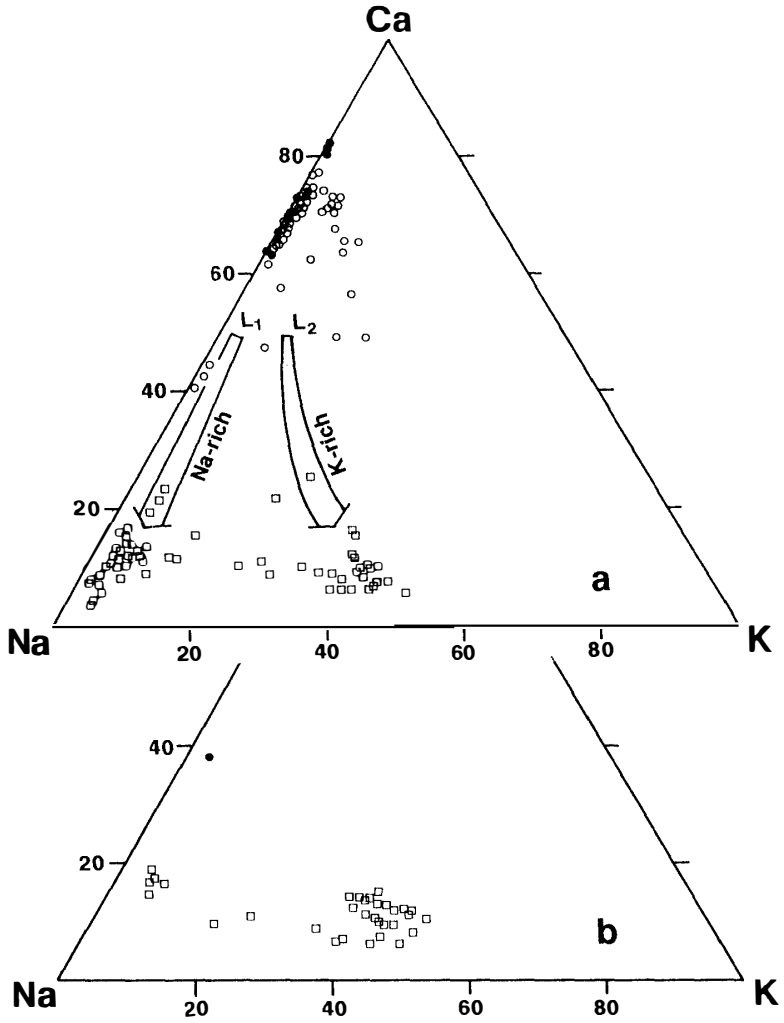

Fig. 6. Ca-Na-K plot (atomic%) of rhyolitic glass (open squares, a), plagioclase (solid circles, a), and fine-grained intergrowth of plagioclase and silica (open circles, a) in silicate inclusions in chadacrystic olivine grains, and rhyolitic glass (open squares, b) and plagioclase (solid circle, b) in oikocrystic pyroxene grains. The Na-rich or K-rich rhyolitic glass was produced from melt L_1 or L_2 by fractional crystallziation of the intergrowth of plagioclase and silica, which are shown by the Na-rich and K-rich trends, respectively (see text).

ular ratios. The intergrowth is various mixtures of calcic plagioclase and qaurtz with minor amounts of rhyolitic glass components.

4.7. Silica-predominant glass

Silica-predominant glass occurs in close association with the fine-grained intergrowth of plagioclase and silica in some silicate inclusions in chadacrystic olivine grains (Fig. 1n). It has rounded or ellipsoidal outlines and always contains small amounts of feldspar components (Table 3). Its normative compositions are plotted in Fig. 7; the normative plagioclase (An+Ab) component is about 5–15 mol% and poor in the normative orthoclase component except for rare cases. The silica-predominant glass also contains a small amount of a normative corundum component (Table 3).

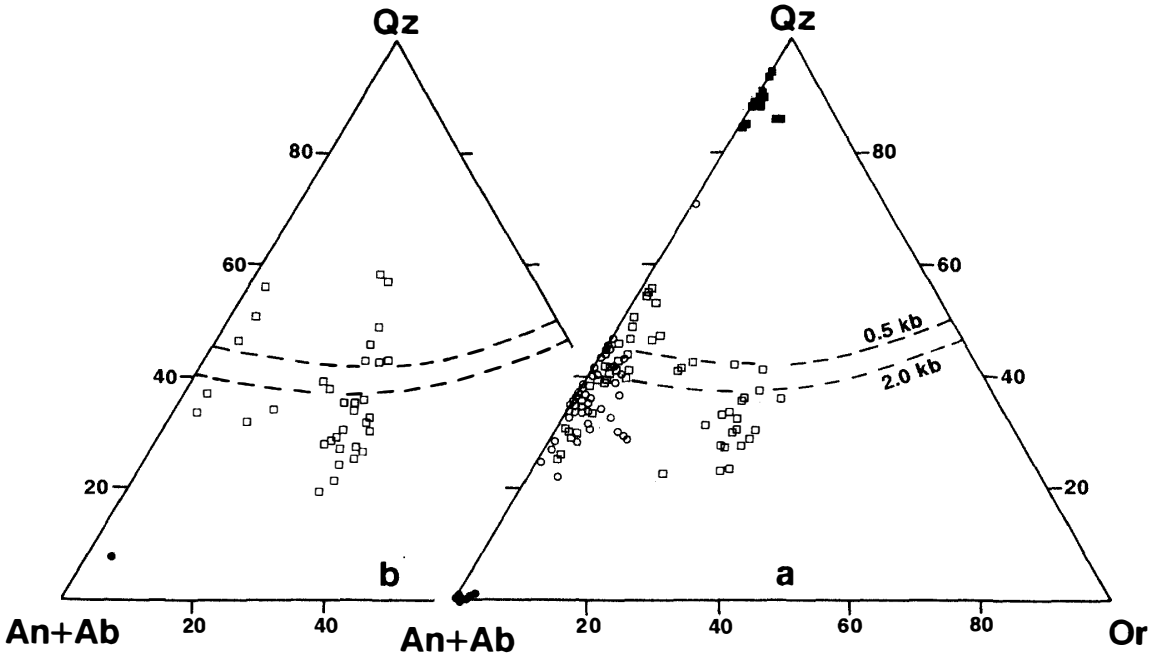

Fig. 7. Normative compositions (mol%, An: $CaSi_2Al_2O_8$, Ab: $NaSi_3AlO_8$, Or: KSi_3AlO_8, Qz: Si_4O_8) of rhyolitic glass (open squares, a), plagioclase (solid circles, a), fine-grained intergrowth of plagioclase and silica (open circles, a), and silica-predominant glass (solid squares, a) in silicate inclusions in chadacrystic olivine grains, and rhyolitic glass (open squares, b) and plagioclase (solid circle, b; this plagiolcase is contaminated by surrounding rhyolitic glass) in silicate inclusions in oikocrystic pyroxene grains. Dashed lines are cotectic lines of the Ab-Or-Silica-H_2O system under 50 Mpa (0.5 kb) and 200 MPa (2.0 kb) of water vapor pressure (TUTTLE and BOWEN, 1958).

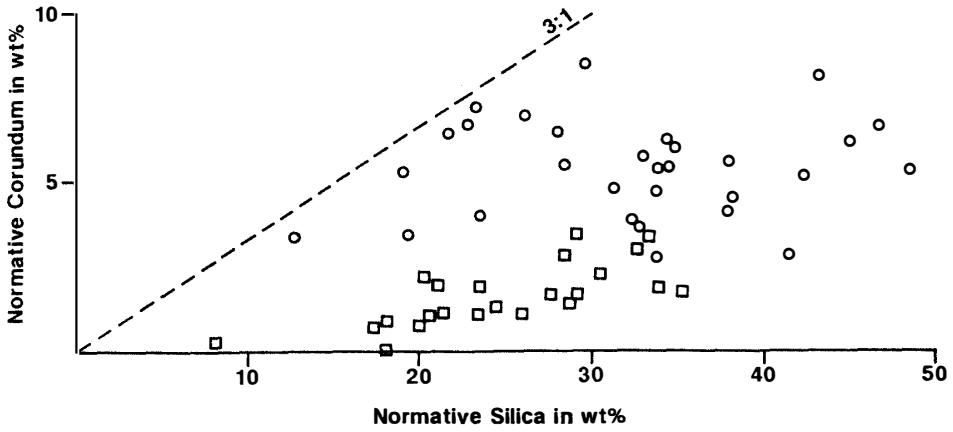

Fig. 8. Normative silica and corundum contents of Na-rich rhyolitic glass (open circles) and K-rich rhyolitic glass (open squares) in silicate inclusions in chadacrystic olivine grains. A line with a wt% ratio of 1/3 is shown for reference.

4.8. Chromite and spinel

Chromite is euhedral or subhedral and occurs as inclusions in chadacrystic olivine and oikocrystic pyroxene grains, and directly in contact with maskelynite. Chromite in chadacrysts shows chemical zoning from Cr-rich cores to Al-rich rims (trend AB in Fig. 9b). Chromite in oikocrysts also shows similar zoning from Cr-rich cores to Al-rich rims (trend CD in Fig. 9a), but trend CD is richer in Cr than trend AB of chromite in chadacrysts. Rare chromite in oikocrysts is rich in TiO_2 (Fig. 9a), and similar in composition to that in contact with maskelynite. Chromite near or in contanct with maskelynite shows remarkable compositional zoning (trend EF in Fig. 9a) from Cr-rich cores to Ti-rich rims with nearly constant Al_2O_3, as shown in Fig. 10. The Cr-rich cores (E in Fig. 9a) are similar in Cr_2O_3, Al_2O_3, and TiO_2 contents to the chromite of trend CD in oikocrysts, and rapidly change their composition towards the rims rich in TiO_2 (Fig. 10). As shown in Fig. 11, chromite in the three trends shows normal Mg-Fe zoning from magnesian cores to ferroan rims. However, trend CD is the most magnesian, and trend AB is less magnesian than trend CD and within the compositional range of trend EF. All chromites in Y-793605 contain V_2O_5 of about 0.5 wt% (Table 2) and seem not to differ in V_2O_5 content among the three trends. The MnO content of chromite ranges from 0.2 to 0.8 wt% (Table 2), but there is no systematic

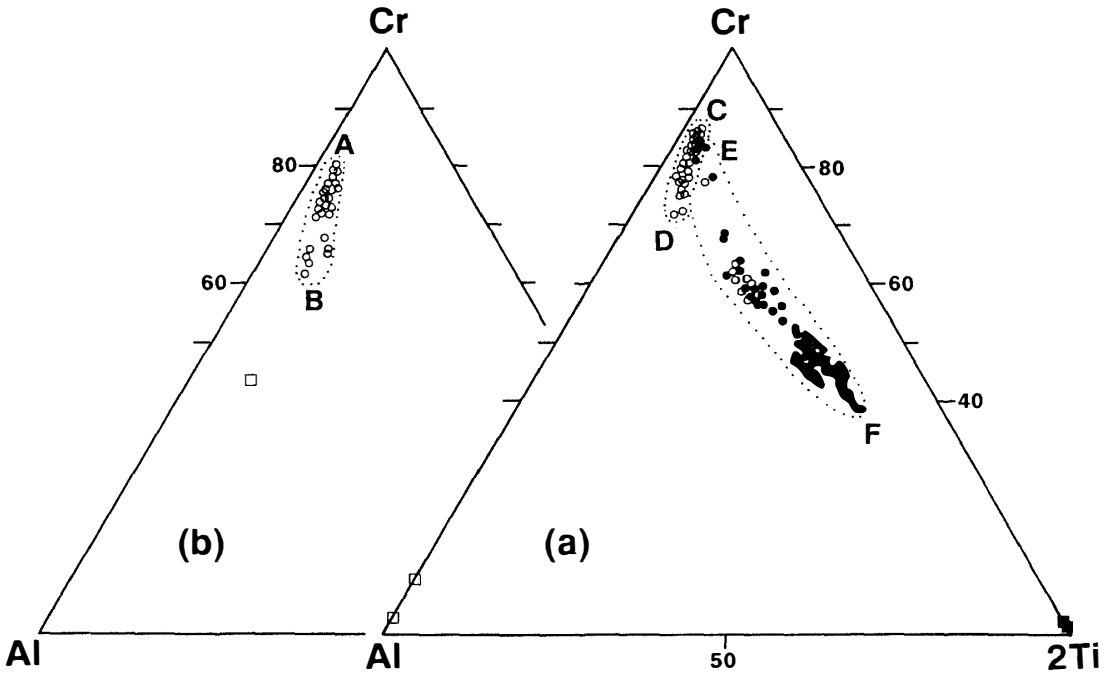

Fig. 9. Cr-Al-2Ti plot (atomic%) of chromite in oikocrystic pyroxene (open circles, a), in contact with or near maskelynite (solid circles, a), and in chadacrystic olivine (open circles, b). Cr-rich spinel in silicate inclusions in chadacrystic olivine grains (open squares, b) and spinel in silicate inclusions in oikocrystic pyroxene grains (open squares, a) are also plotted for reference. Compositional trends of chromite in chadacrystic olivine grains, in oikocrystic pyroxene grians, and in contanct with or near maskelynite are shown by AB, CD, and EF, respectively.

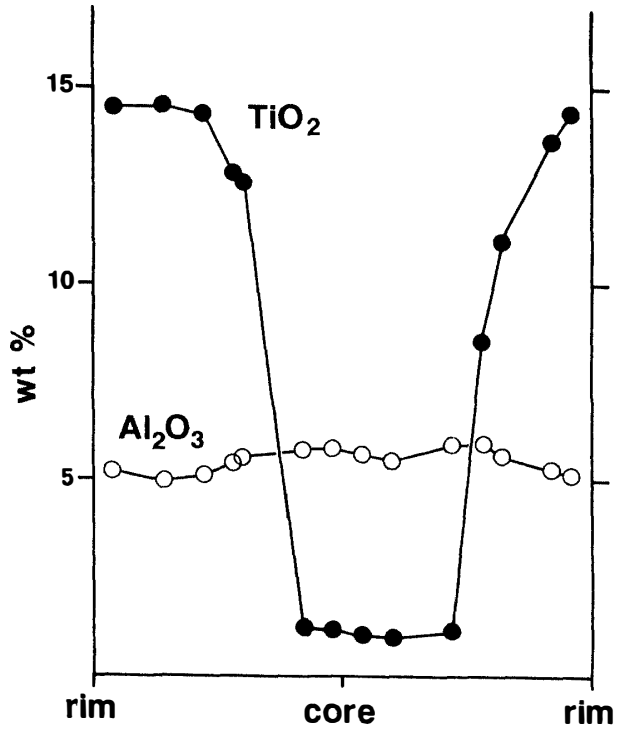

Fig. 10. Compositional zoning of a chromite grain with a diameter of 156 μm, which is in contact with maskelynite.

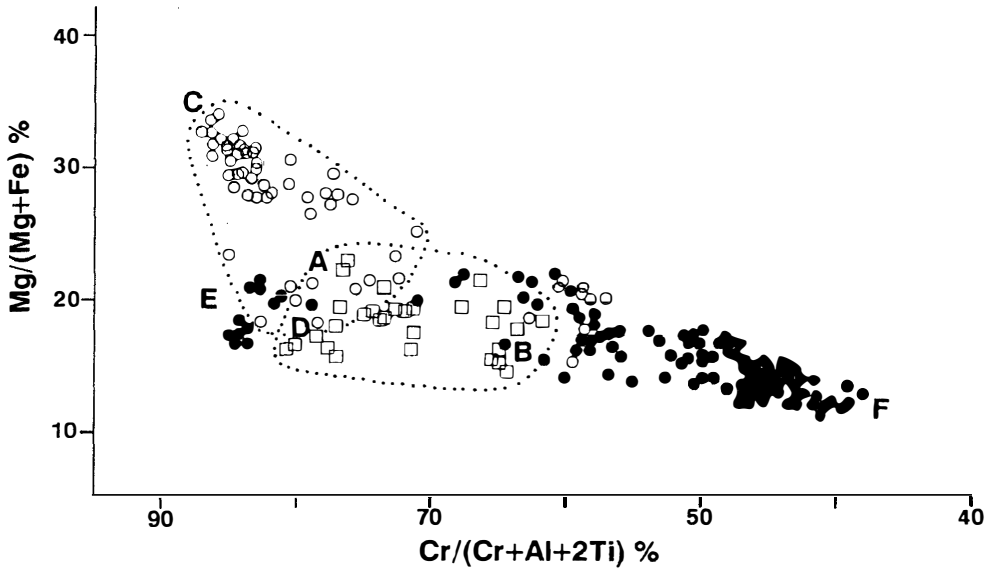

Fig. 11. Mg/(Mg+Fe) atomic% of chromite in chadacrystic olivine grains (open squares with trend AB), in oikocrystic pyroxene grains (open circles with trend CD), and near or in contact with maskelynite (solid circles with trend EF), are plotted against their Cr/(Cr+Al+2Ti) atomic%.

difference in MnO content among the three trends. The ZnO content of chromite is lower than the detection limit (0.1 wt%). The NiO content is 0.0–0.3 wt%.

Spinel occurs in close association with ilmenite in silicate inclusions in chadacrystic olivine and oikocrystic pyroxene grains (Fig. 1l, p). They are aluminous and poor in TiO_2 (Table 3, Fig. 9).

4.9. Ilmenite and sulfide

Ilmenite occurs near maskelynite as isolated crystals or in close association with chromite F. It contains MgO of 4–6 wt%, Cr_2O_3 of 0.2–0.6 wt%, MnO of 0.5–0.9 wt%, V_2O_5 of 0.1–0.4 wt%, and NiO of 0.0–0.2 wt% (Table 2). Ilmenite rarely includes small grains or lamellae of baddeleyite (Fig. 1i). Sulfide occurs near maskelynite and is pyrrhotite, with the Ni content of 1–3 wt% and Co of 0.1–0.3 wt% (Table 4). Sulfide is rarely found in silicate inclusions (Fig. 1l).

4.10. Glassy substance in shock-induced crushed zone

Glassy substance occurs locally in a shock-induced crushed zone (Fig. 1s, t). The

Table 4. Chemical compositions of pyrrhotite (Pyrr) in Y-793605.

	Pyrr	Pyrr	Pyrr
Fe	60.76	60.17	58.15
Co	0.18	0.12	0.27
Ni	1.32	1.55	2.35
S	36.70	37.01	37.53
Total	98.96	98.85	98.30

Table 5. Chemical compositions of magmesian olivine (mOl), glassy substances (Melt) occurring in shock-induced crushed zone and magnesian olivine (mOl) and pyroxene (mPx) occurring in fusion crust. The bulk composition of Y-793605 (Bulk; WARREN and KALLEMEYN, 1997) is shown for reference.

	Crushed zone				Fusion crust	
	mOl	Melt	Melt	Bulk	mOl	mPx
SiO_2	40.17	41.11	40.17	45.35	42.74	56.43
TiO_2	0.06	0.37	0.50	0.35	0.05	0.09
Al_2O_3	0.36	3.36	3.10	2.32	0.55	0.35
Cr_2O_3	0.63	0.81	0.90	0.01	0.06	0.85
FeO	14.29	24.24	24.73	19.68	6.48	8.49
MnO	0.44	1.09	0.53	0.48	0.44	0.38
MgO	43.90	23.88	26.80	26.20	49.46	31.38
CaO	0.25	3.71	2.59	4.06	0.65	1.25
Na_2O	0.12	0.63	0.55	0.354	0.13	0.05
K_2O	0.05	0.08	0.04	0.025	0.00	0.00
Total	100.27	99.28	99.90	99.83	100.57	99.25

chemical compositions is shown in Table 5, and it is similar to the bulk composition of Y-793605 obtained by WARREN and KALLEMEYN (1997), although the glassy substance is poorer in SiO_2 and more enriched in olivine components than the latter. It may have been locally produced from crushed materials of the host lithology by melting due to local stress concentration during an impact shock.

4.11. Secondary alteration products due to weathering

In Y-793605, olivine, chromite, ilmenite, and pyrrhotite have suffered weathering alteration along thier rims and fractures in them (Fig. 1b, e, f, h, j, k, r, v, w), although pyroxene and maskelynite seem not to have experienced secondary altration. All phosphates in Y-793605 seem to have wholly altered by weathering. All of the alteration products are very fine-grained and submicroscopic in grain size. The secondary alteration products are grouped into three chemical types on the basis of chemical compositions, Fe-K-S, Si-Fe-Mg, and Si-Al-Fe types (Table 6, Fig. 12). The alteration products are often enriched in K_2O and have K/(Ca+Na+K) atomic ratios higher than 0.7.

4.11.1. Fe-K-S type alteration products

Opaque minerals such as chromite, ilmenite, and pyrrhotite, as well as phosphates, have partly or wholly altered by weathering to Fe-K-S-(P)-rich alteration products along their rims and fractures (Fig. 1e, f, h, j, r). They are always enriched in FeO (or Fe_2O_3) and SO_3, and often in K_2O and P_2O_5 (Table 6). The SO_3 content ranges from 2 to 30 wt% (mostly 20–25 wt%), suggesting that iron sulfates are predominant components of the alteration products. The K_2O content is variable, up to 6.5 wt% (mostly 2–6 wt%), but the CaO and Na_2O contents are usually lower than 1.0 wt%

Table 6. Chemical compositions of alteration products in Y-793605. The estimated precursors of the alteration products are shown in the first line; they are non-rhyolitic glass (Gl), olivine (Ol), opaque minerals (chromite, ilmenite, or pyrrhotite) and phosphates (Opaq), and their mixtures (Mix). Veinlets (Vein) which cut silicates and/or opaque minerals are also alteration products. The chemical types of weathering alteration products are shown in the second line.

	Gl	Gl	Ol	Ol	Mix	Mix	Opaq	Opaq	Vein	Vein
	Si-Al-Fe		Si-Fe-Mg		Mix		Fe-K-S			
SiO_2	59.04	65.74	64.17	44.91	33.28	27.44	0.00	10.79	6.20	12.13
TiO_2	0.37	0.46	0.00	0.00	0.16	0.24	0.12	0.08	0.02	0.00
Al_2O_3	13.32	8.02	0.26	0.12	4.64	4.96	0.13	0.22	0.24	3.72
Cr_2O_3	0.00	0.13	0.19	0.45	0.27	0.40	0.37	0.27	0.67	0.93
FeO	9.01	4.58	11.36	23.68	21.45	26.46	42.92	36.07	35.27	34.36
MnO	0.03	0.00	0.00	0.30	0.00	0.00	0.00	0.00	0.04	0.00
MgO	2.48	1.39	4.04	18.24	0.88	0.62	0.10	0.10	0.24	0.11
CaO	0.32	0.09	0.16	0.13	0.17	0.25	0.00	0.11	0.11	1.79
Na_2O	0.07	0.00	0.00	0.01	0.43	0.93	0.14	0.74	0.60	0.92
K_2O	1.61	1.08	0.64	0.24	4.06	5.21	6.10	5.88	3.63	3.39
P_2O_5	0.07	0.12	0.68	0.17	2.62	1.69	0.07	2.60	1.77	1.62
SO_3	0.55	0.94	3.05	1.31	12.14	15.37	27.55	21.64	24.20	20.36
Total	86.88	82.53	84.54	89.54	80.10	83.61	77.48	78.50	72.98	79.34

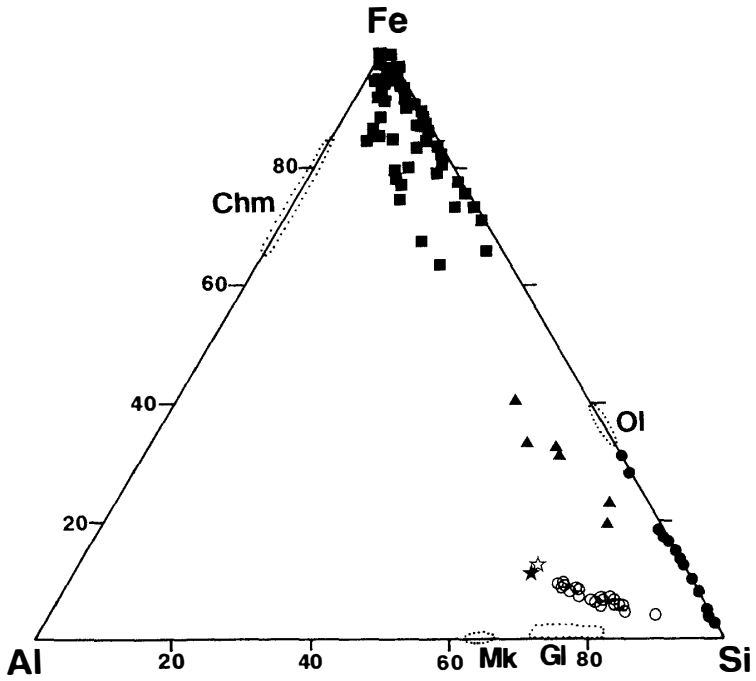

Fig. 12. Fe-Al-Si plot (atomic%) of chemical types of secondary alteration products, Fe-K-S type (solid squares), Si-Fe-Mg type (solid circles), Si-Al-Fe type (open circles), and mix type (solid triangles). Compositional ranges of chromite (Chm), olivine (Ol), maskelynite (Mk), and rhyolitic glass and fine-grained intergrowth of plagioclase and silica in silicate inclusions (Gl) are shown for reference. Open star is non-rhyolitic glass, and solid star is ferric Fe pyrophyllite ($Fe_{1.3}Al_{2.7}Si_8O_{20}(OH)_4$).

(mostly less than 0.3 wt%). The P_2O_5 content is also variable, up to 30 wt% (mostly 1–5 wt%). The contents of TiO_2, Cr_2O_3, Al_2O_3, and SiO_2 are also variable, sometimes TiO_2 and Cr_2O_3 ranging up to more than 10 wt%.

Veinlets due to weathering alteration, a few μm in width, often cut silicate minerals (Fig. 1v, w). The alteration veinlets sometimes merge into massive alteration products which occur around opaque minerals (Fig. 1w). Their chemical compositions (Table 6) are similar to the alteration products of opaque minerals and are Fe-K-S type.

4.11.2. Si-Fe-Mg type alteration products

Olivine has partly altered along their grain rims and fractures in it (Fig. 1b). Most of the alteration products of olivine are enriched in silica (40–70 wt%) and poor in Al_2O_3 (<1 wt%) (Table 6). The FeO content ranges from 2 to 24 wt%, the MgO content is from 0.5 to 20 wt%, and there is a tendency that the MgO content decreases with decreasing FeO. The K_2O and P_2O_5 contents are from 0.2 to 2.5 wt%, and the SO_3 content is 1–10 wt%. They are Si-Fe-Mg type, and are plotted between olivine and the Si-apex in Fig. 12.

4.11.3. Si-Al-Fe type alteration products

Si-Al-Fe-rich alteration products occur near maskelynite, and seem to replace the non-rhyolitic glass (Fig. 1k). They are massive and look like an amorphous material

(Fig. 1v), but show low birefringence under an optical microscope with crossed Nicols, suggesting that they are cryptocrystalline. The SiO_2 content is 54–70 wt%, Al_2O_3 is 5–14 wt%, and FeO is 4–9 wt%, with minor contents of TiO_2 (0.3–1.0 wt%), MgO (0.8–3.0 wt%), K_2O (0.5–2.3 wt%), and SO_3 (0.4–1.0 wt%) (Table 6). The other components (CaO, Na_2O, Cr_2O_3, and P_2O_5) are less than 0.5 wt%. As shown in Fig. 12, the chemical compositions of Si-Al-Fe type are plotted between the non-rhyolitic glass and the Si apex.

4.11.4. Mix-type alteration products

The three chemical types of alteration products have their proper compositional ranges as shown in Fig. 12. However, sometimes the two or three types occur in mixing way and they are plotted between them (Fig. 12). Some of Si-Al-Fe type are mixed with Fe-K-S type, and enriched in SO_3 (8–16 wt%), K_2O (2–6 wt%), and P_2O_5 (1–3 wt%), in addition to Al_2O_3 (2–5 wt%) and silica (20–40 wt%) (Table 6).

5. Discussion

5.1. Compositional trends of chromite

Chromite in Y-793605 shows three compositional trends according to its occurrence. Chromite in chadacrystic olivine grains has trend AB, and shows zonation from A to B, whereas chromite in oikocrystic pyroxene grains has trend CD and shows zonation from C to D. The poikilitic texture of Y-793605 suggests that the chadacrystic olivine crystallized prior to the oikocrystic pyroxene, and the corroded outlines of the chadacrystic olivine grains indicate that the olivine reacted with the coexisting magma to produce the oikocrystic pyroxene. Therefore, chromite AB must have crystallized prior to chromite CD. However, there is a compositional gap between chromites AB and CD; chromite B is not continuous in composition to chromite C, as shown in Fig. 9. The Mg/(Mg+Fe) ratios (mg ratios, hereafter) of chromite AB are lower than those of chromite CD (Fig. 11), indicating again that chromite B is different in composition from chromite C. These suggest that there was a gap in compositions between two magmas which crystallized chromites of trends AB and CD, respectively. These relationships are the same as those for ALHA77005 (IKEDA, 1994), and IKEDA (1994) suggested that a magma mixing model may explain the compositional relationships for chromite trends.

Chromite which is in contanct with maskelynite has trend EF, and the cores (E) of chromite coincide with trend CD (Fig. 9), suggesting that the magma for chromite EF may be comagmatic with that for chromite CD. Chromite F often coexists with ilmenite and maskelynite, indicating that they are the late-stage crystallization products. The mg ratios of chromite CD are continuous to those of chromite EF (Fig. 11), supporting their comagmatic crystallization. However, strictly speaking, the mg ratios of chromite E seem to be slightly lower than those of chromite CD (Fig. 11). This discrepancy may be explained by a concept that chromite CD was included in oikocrystic pyroxene grains to prevent Mg-Fe diffusion between chromite CD and the residual magma, whereas chromite EF could easily exchange its Mg with Fe of the coexisting residual magma.

5.2. Crystallization and origin of silicate inclusions

5.2.1. Crystallization of silicate inclusions in chadacrystic olivine

Silicate inclusions in chadacrystic olivine grains crystallized probably at first olivine on the wall of silicate inclusions, and then aluminous low-Ca pyroxene, followed by fassaitic pyroxene, ilmenite, spinel, and sulfide. The intergrowth of plagioclase and silica crystallized at the last stage of crystallization along with a silica-predominant glass which was probably a silica mineral before an impact shock took place.

Pyroxenes in silicate inclusions are similar in major element compositions (Ca, Mg, and Fe) to the pyroxenes of the host lithology (Fig. 3). However, the minor element contents (Al_2O_3, Cr_2O_3, and TiO_2) of the inclusion pyroxenes are decidedly different from the pyroxenes of the host lithology as shown in Fig. 4, suggesting that the inclusion pyroxenes crystallized from an Al-Ti-rich and Cr-poor magma, which was different from a magma for the host lithology.

The intergrowth of plagioclase and silica may have crystallized under a rapidly cooling condition to produce the fine-grained intergrowth texture. The plagioclase of the intergrowth is $An_{63\text{-}83}$ (Fig. 6) and more calcic than the maskelynite of the host lithology, suggesting again that the melts of silicate inclusions were different from the magma of the host lithology.

The silica-predominant glass occurs in close association with the intergrowth of plagioclase and silica, and this glass, as well as the silica of the intergrowth, was a silica mineral which crystallized from the melts of silicate inclusions together with the plagioclase. Probably the inclusion melts may have saturated with both silica and plagioclase at the same time. Although maskelynite occurs as the main mineral in the host lithology, any silica mineral never occurs in the host lithology. The magma for the host lithology may have undersaturated with silica components, supporting the difference in composition between the inclusion melts and the magma for the host lithology.

The rhyolitic glass are plotted around the cotectic lines of the granitic system in Fig. 7, and it may have cosaturated with silica and plagioclase components. As shown in Fig. 6, the rhyolitic glass was produced from inclusion melts by fractional crystallization of the intergrowth of plagioclase and silica. As the inclusion melts crystallized calcic plagioclase of $An_{80\text{-}83}$, they may have a normative plagioclase component around An_{50} prior to the crystallization of the intergrowth of plagioclase and silica, because a melt with normative An_{50} coexists with plagioclase of An_{82} (BOWEN, 1913). In Fig. 6, the inclusion melts are designated as L_1 for the Na-rich rhyolitic glass and L_2 for the K-rich rhyolitic glass; the inclusion melts such as L_1 and L_2 may have saturated with both plagioclase and silica, have had a normative plagioclase component around An_{50}, and have been heterogeneous in Na/K ratios ranging from L_1 to L_2. In addition to these, as the rhyolitic glass, especially Na-rich one, often contains normative corundum components (Table 3, Fig. 8), the inclusion melts may have been peraluminous. This peraluminous feature is consistent with the crystallization of aluminous pyroxenes in silicate inclusions in chadacrystic olivine grains.

5.2.2. Crystallzation of silicate inclusions in oikocrystic pyroxene

Silicate inclusions in oikocrystic pyroxene grains never include the intergrowth of plagioclase and silica, and their crystallization seems to be simple in comparison

to the silicate inclusions in chadacrystic olivine grains. They crystallized pyroxene, ilmenite, and rarely sodic plagioclase and spinel. The rhyolitic glass was residual melts which have quenched under a rapidly cooling condition. The K-rich rhyolitic glass is more abundant than the Na-rich one, and this is a contrast to the silicate inclusions in chadacrysts among which the Na-rich rhyolitic glass is more abundant than the K-rich one (Fig. 6).

There are two types of the inclusion pyroxenes in oikocrysts, Al-rich and Al-poor. The Al-rich pyroxenes are very similar in major and minor element contents to those in silicate inclusions in chadacrysts. However, the Al-poor pyroxenes are similar to the pigenitic pyroxenes of the host lithology, but the former are more ferroan than the latter (Fig. 3).

5.2.3. Origin of silicate inclusions

The rhyolitic glass and the inclusion melts such as L_1 and L_2 in Fig. 6 were often peraluminous and saturated with both silica and plagioclase components. The host lithology of Y-793605 never includes silica minerals, and the oikocrystic pyroxenes are not aluminous (Fig. 4). These line of evidence suggests that the magma for chadacrystic olivines is different from the magma for oikocrystic pyroxenes. This difference may be explained by a magma mixing model; the magma which was crystallizing olivines was originally enriched in silica and alumina and probably had a low mg ratio , and then this magma mixed with a magma which did not saturate with silica and plagioclase components, was not so much peraluminous, and had a higher mg ratio. The mixed magma reacted the olivines to produce oikocrystic pyroxenes, resulting in the poikilitic texture of Y-793605. However, the mixing was not complete at least in the early stage of the mixing, and the oikocrystic pyroxenes included two types of the magmas as magmatic inclusions during their crystallization in the magma reservoir.

As already discussed in the previous section, the rhyolitic glass has various Na/K ratios, and the magmas which crystallized chadacrystic olivine and oikocrystic pyroxene grains should have been heterogeneous in Na/K ratios. The Na-rich rhyolitic glass is more abundant than the K-rich one in chadacrysts whereas the situation is reverse in silicate inclusions in oikocrysts. This various Na/K ratios may be explained by the magma mixing model; the two magmas may have had a higher Na/K ratio and a lower Na/K ratio, respectively. For this case, multiple magma mixing should have taken place during the crystallization of olivines, because the inclusion melts (such as L_1 or L_2 in Fig. 6) in the chadacrystic olivines have various Na/K ratios.

Magmatic silicate inclusions occur in other martian meteorites, and they are generally considered to represent fractionated melts of the parental magmas of the host lithologies (FLORAN *et al.*, 1978; TREIMAN, 1985; JAGOUTZ, 1989; HARVEY and MCSWEEN, 1992; HARVEY *et al.*, 1993). However, the magma mixing model for their origin may be a likely hypothesis at least for lherzolitic shergottites (IKEDA, 1994).

5.3. Crystallization of Y-793605

Crystallization of Y-793605 is summarized in Fig. 13. The original Y-793605 magma was crystallizing olivines and chromites of trend AB, and then magma mixing took place, resulting in corrosion of the olivines by reaction with the mixed magma.

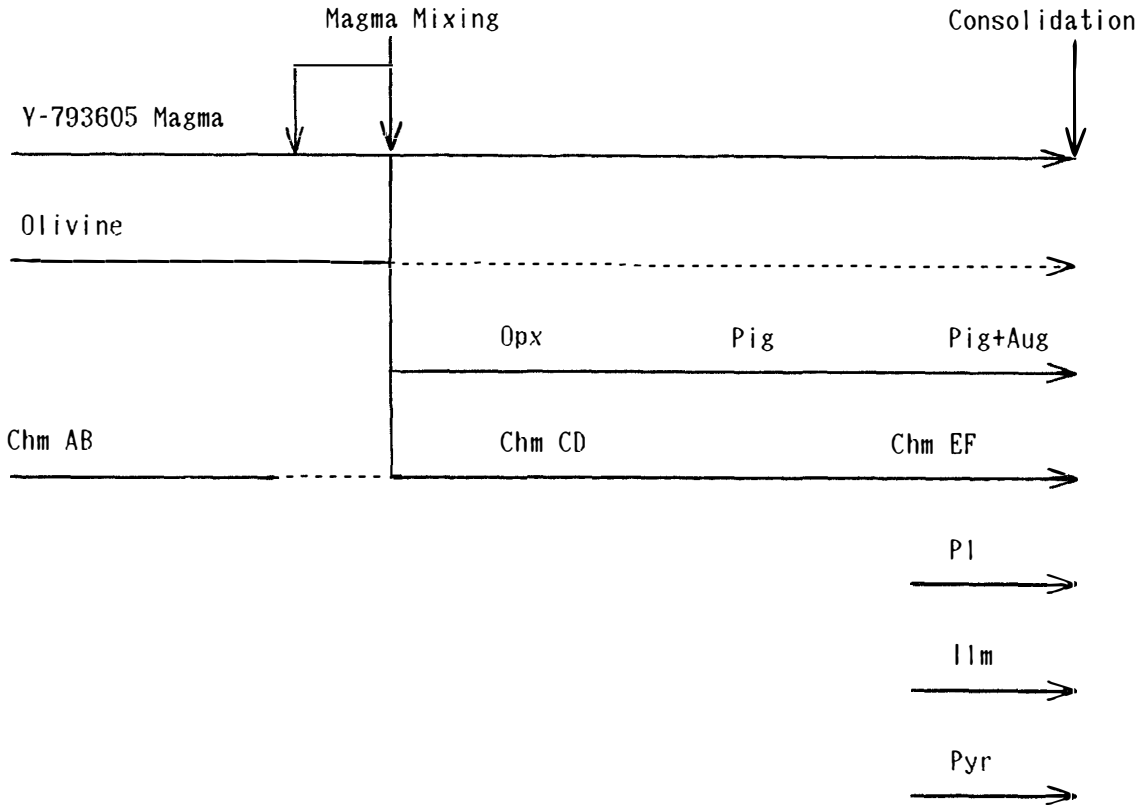

Fig. 13. Crystallization sequence of Y-793605. The original Y-793605 magma crystallized at first olivine (Ol) and chromite (Chm) AB, and then experienced magma mixing. After the mixing, olivine was corroded by reaction with the mixed magma to produce low-Ca pyroxene, resulting in the poikilitic texture of Y-793605. The oikocrystic low-Ca pyroxene was first orthopyroxene (Opx) and then followed by pigeonite (Pig). Chromite CD also crystallized from the magma to be included in oikocrystic pyroxene. Plagioclase (Pl, it was tranformed to maskelynite by a later impact shock) crystallized together with pigeonite, augite (Aug), chromite with trend EF, ilmenite (Ilm), pyrrhotite (Pyr), and probably phosphates, at the last stage of crystallization.

The mixed magma at first crystallized magnesian low-Ca pyroxene (orthopyroxene), chromite CD, and then pigeonite, which included poikilitically corroded olivine grains and chromites of trend CD. As degrees of crystallization proceeded, the mixed magma was enriched in Ti, Ca, alkalies, Si, and so on. In the late stage of crystallization the magma crystallized augite, chromite of composition F, plagioclase, ilmenite, pyrrhotite, and probably phosphates. Application of the two-pyroxene geothermometer (LINDSLEY and ANDERSEN, 1983) for Y-793605 augite just in contact with pigeonite gives an equilibrium temeparture of about 1220°C.

5.4. Impact shock

Planar fractures are common in Y-793605, which displace the mineral grains such as pyroxene and chromite in distance up to 200 μm (Fig. c, r, u). These planar fractures are often found in oikocrystic pyroxene grains, and this may be due to more brittle nature of pyroxene and chromite in comparison to olivine.

A shock-induced crushed zone was found in one thin section (51-1), where the minerals of the host lithology were crushed into fine -grained aggregates (Fig. 1s). Although glassy substance occurs locally in the crushed zone (Fig. 1s, t), most of fine-grained aggregates seem not to have experienced whole melting. Small magnesian olivine grains occur in the fine-grained aggregates, suggesting that the fine-grained aggregates were partially melted and the magnesian olivine crystallized from the melts. There is no shock melt pocket in the thin sections studied. These are a contrast to impact shock features of ALHA77005; shock melt pockets and shock melt veins are common in ALHA77005 (IKEDA, 1994; TREIMAN *et al.*, 1994). Maskelynite occurs as the main mineral in Y-793605, although plagioclase melt is common in ALHA77005 instead of maskelynite (IKEDA, 1994). These indicate that shock stage of Y-793605 is lower than that of ALHA77005 and may be S5 (30–55 GPa, STÖFFLER *et al.*, 1991; BISHOP and STÖFFLER, 1992).

Judging from the occurrence of the non-rhyolitic glass in Y-793605 (Fig. 1j), it could be mesostasis glass. However, the normative feldspar composition of the glass is $An_{52}Or_5$, and can not be in equilibriun with the coexisting plagioclase (now maskelynite) of $An_{30\text{-}58}$; plagioclase of An_{50} or An_{40} coexists with a melt of An_{13} or An_8 for the plagiolcase system under 0.1 MPa (one atmospheric pressure) (BOWEN, 1913), respectively. The non-rhyolitic glass may not be mesostasis and probably represents impact shock melts of mixtures of plagioclase, pyroxene, and mesostasis. In this case, silica-rich precursors such as mesostasis is needed because the non-rhyolitic glass contains a normative quartz component. Another hypothesis is that it is shock-melt glass of a kind of amphibole. Further study of the non-rhyolitic glass is necessary for its origin.

5.5. Weathering alteration

The alteration products in Y-793605 are grouped into three chemical types, Fe-K-S, Si-Al-Fe, and Si-Fe-Mg types on the basis of their chemical compositions. This indicates that each type was not mixed by one another and the weathering alteration took place locally in the Y-793605 meteorite. The Fe-K-S type may consist mainly of iron sulfates and K-bearing sulfates with variable amounts of silica such as chalcedony or amorphous silica. The Fe-K-S type occurs often as veinlets, suggesting that some kinds of fluid reacted with opaque minerals (chromite, ilmenite, and pyrrhotite) and phosphates to produce the veinlets.

The Si-Al-Fe type may have been produced from non-rhyolitic glass (Fig. 12), and seems to be mixtures of an aluminosilicate such ferric Fe pyrophyllite and silica such as chalcedony or amorphous silica. The Si-Al-Fe type occurs commonly near maskelynite, but maskelynite is very fresh and has never altered in Y-793605. The non-rhyolitic glass may be apt to suffer weathering alteration by unknown processes. The formation of the Si-Al-Fe type may have taken place at the same times as that of the Fe-K-S type, because the veinlets of the Fe-K-S type sometimes merge into the Si-Al-Fe type (Fig. 1v).

The Si-Fe-Mg type was produced from olivine by introduction of silica and loss of MgO and FeO. Sometimes this type occurs along veinlets of the Fe-K-S type which cut some olivine grains. Thus, the Si-Fe-Mg type has probably been produced after

the fomation of the Fe-K-S type.

The formation of the three types was caused by introduction of SiO_2, K_2O, and water, and by loss of TiO_2, Cr_2O_3, MgO, CaO, P_2O_5, and Na_2O during thier alteration. The weathering alteration may have taken place either on Mars or on Earth. Textural evidence shown in Fig. 1r indicates that the alteration took place after the formation of planar fractures; Fe-K-S type alteration products completely surround the chromite which was cut by a planar fracture. Fig. 1x also suggests that a veinlet of the Si-Mg-Fe type cut the fusion crust. Therefore, the weathering alteration may have taken place on the Earth after the formation of the fusion crust. Secondary alteration products in Antarctic meteorites are sometimes rich in Si, Fe, S, and K (GOODING, 1989), and this is consistent with the conclusion that the weathering alteration of Y-793605 took place in Antarctica.

Olivine and chromite in ALHA77005 have also experienced weathering alteration (SMITH and STEELE, 1984). The alteration products of olivine and chromite reported by SMITH and STEEL (1984) are very similar to those in Y-793605, corresponding to the Si-Fe-Mg and Fe-K-S types, respectively. They concluded that the alteration of ALHA77005 took place in Antarctica, and it is consistent with the conclusion above stated for Y-793605. However, the degree of the alteration seem to be higher for Y-793605, because phosphates have partially altered in ALHA77005 although they have completely altered in Y-793605.

5.6. Comparison with ALHA77005 and LEW88516

TREIMAN *et al.* (1994) concluded that LEW 88516 is very similar in mineral composition, bulk composition, and texture to ALHA77005. Y-793605 also is very similar to ALHA77005 and LEW88516 (MIKOUCHI and MIYAMOTO, 1996). However, there are several differences between them; (1) Olivines in ALHA77005 are brownish under an optical microscope with open Nicol (OSTERTAG *et al.*, 1984; SMITH and STEELE, 1984), whereas olivines in Y-793605 are not brownish but pale yellow. The brown olivines in ALHA77005 are mostly $Fa_{25\text{-}30}$ (IKEDA, 1994), and are nearly the same as the chadacrystic olivines in Y-793605, although the ferroan olivines ($Fa_{31\text{-}36}$) in contact with the maskelynite in Y-793605 are more ferroan than the brown olivines in ALHA77005. Olivines in poikilitic area of LEW88516 are $Fa_{26\text{-}38}$, and those in non-poikilitic area are $Fa_{30\text{-}40}$ (HARVEY *et al.*, 1993). The bimodal compositions of olivines in LEW88516 are similar to those in Y-793605, although olivines in LEW88516 are more ferroan as a whole than those in Y-793605. (2) ALHA77005 includes many shock melt pockets and shock melt veins (MCSWEEN and STÖFFLER, 1980; IKEDA, 1994), and LEW88516 also includes them in non-poikilitic area (HARVEY *et al.*, 1993). However, Y-793605 has rare shock-melt pockets. (3) Maskelynite seems not to occur in ALHA77005, and instead of it glass of plagioclase compositions with plagioclase rims is common (IKEDA, 1994). On the other hand, maskelynite occurs in Y-793605, and no plagioclase glass there. (4) Olivine, chromite, ilmenite, and sulfide in Y-793605 experienced weathering alteration, whereas those in ALHA77005 seem to have suffered less degrees of weathering. In addition, veinlets due to weathering are common in Y-793605 although they are rare in ALHA77005.

Conclusively, Y-793605 is very similar in mineralogy and texture to ALHA77005

and LEW88516, and more similar to LEW88516. However, shock effects for Y-793605 are the weakest among the three. Weathering effects in Y-793605 are the most intense among them. The compositional range of olivines in Y-793605 is intermediate between the other two. These suggest that Y-793605 is not pair with ALHA77005 and LEW88516.

6. Conclusions

(1) Chromites in Y-793605 have different compositional ranges according to their occurrence; chromite in chadacrystic olivines is Al-rich and Ti-poor, that in oikocrystic pyroxenes is Cr-rich and Ti-poor, and that in contanct with maskelynite is Ti-rich.

(2) Magmatic silicate inclusions in chadacrystic olivines cosaturated with silica and plagioclase (An_{63-83}) and was often peraluminous, and the pyroxenes are rich in Al and Ti, but poor in Cr.

(3) Magmatic inclusions in oikocrystic pyroxenes include two types of pyroxenes, Al-rich and Al-poor. The K-rich rhyolitic glass is more abundant than the Na-rich rhyolitic glass in oikocrystic pyroxenes, and this is a contrast to the silicate inclusions in chadacrystic olivines where the latter is more abundant.

(4) The magma for the host lithology crystallized plagioclase of An_{30-58}, but it was not peraluminous and not saturated with silica. The difference between the inclusion melts and the magma of the host lithology suggests that multiple magma mixing took place between the crystallization stages of chadacrystic olivines and oikocrystic pyroxenes.

(5) Y-793605 experienced an intense impact shock, but the degree for Y-793605 may be lower than those for ALHA77005 and LEW88516.

(6) Y-793605 suffered weathering alteration probably at Antarctica. Olivine and opaque minerals, as well as phosphates, have partially or wholly altered, whereas pyroxene and maskelynite remain unaltered.

Acknowledgments

I thank Drs. H. KOJIMA, P. WARREN, M. MIYAMOTO, and K. YANAI for the organization of the Y-793605 research consortium, Dr. M. MIYAMOTO for critical reading of manuscript, and NIPR for the loan of thin sections of Y-793605.

References

BENCE, A.E. and ALBEE, A.L. (1968): Empirical correction factors for the electron microanalysis of silicates and oxides. J. Geol., **76**, 382–403.

BISHOP, A. and STÖFFLER, D. (1992): Shock metamorphism as a fundamental process in the evolution of planetary bodies: Information from meteorites. Eur. J. Mineral., **4**, 707–755.

BOWEN, N.L. (1913): The melting phenomena of the plagioclase feldspars. Am. J. Sci., **35**, 577–599.

FLORAN, R.J., PRINZ, M., HLAVA, P.F., KEIL, K., NEHRU, C.E. and HINTHORNE, J.R. (1978): The Chassigny meteorite: A cumulate dunite with hydrous amphibole-bearing melt inclusions. Geochim. Cosmochim. Acta, **42**, 1213–1229.

GOODING, J.L. (1989): Significance of terrestrial weathering effects in Antarctic meteorites. Smithson. Contrib. Earth Sci., **28**, 93–98.

HARVEY, R. P. and MCSWEEN, H. Y., Jr. (1992): The parent magma of the nakhlite meteorites: Clues from melt inclusions. Earth Planet. Sci. Lett., **111**, 467–482.

HARVEY, R.P., WADHWA, M., MCSWEEN, H.Y., Jr. and CROZAZ, G. (1993): Petrology, mineral chemistry, and petrogenesis of Antarctic shergottite LEW88516. Geochim. Cosmochim. Acta, **57**, 4769–4786.

IKEDA, Y. (1994): Petrography and petrology of the ALH-77005 shergottite. Proc. NIPR Symp. Antarct. Meteorites, **7**, 9–29.

JAGOUTZ, E. (1989): Sr and Nd isotopic systematics in ALHA77005: Age of shock metamorphism in shergottites and magmatic differentiation on Mars. Geochim. Cosmochim. Acta, **53**, 2429–2441.

KOJIMA, H., MIYAMOTO, M. and WARREN, P. H. (1997): The Yamato-793605 martian meteorite consortium. Antarct. Meteorite Res., **10**, 3–12.

LINDSLEY, D.H. and ANDERSEN, D.J. (1983): A two-pyroxene thermometer. Proc. Lunar Planet. Sci. Conf., 13th, Pt. 2, A887–A906 (J. Geophys. Res., **88** Suppl.)

MCSWEEN, H.Y., Jr. (1994): What we have learned about Mars from SNC meteorites. Meteoritics, **29**, 757–779.

MCSWEEN, H.Y., Jr. and STÖFFLER, D. (1980): Shock metamorphic features in Allan Hills 77005 meteorite. Lunar and Planetary Science XI. Houston, Lunar Planet. Inst., 717–719.

MIKOUCHI, T. and MIYAMOTO, M. (1996): Comparative mineralogy of Antarctic lherzolitic shergottites ALH 77005, LEW 88516, and Y 793605. Meteorit. Planet. Sci., **31**, Suppl., A89–A90.

OSTERTAG, R., AMTHAUER, G., RAGER, H. and MCSWEEN, H.Y., Jr. (1984): Fe^{3+} in shocked olivine crystals of the ALHA77005 meteorite. Earth Planet. Sci. Lett., **67**, 162–166.

SMITH, J. V. and STEELE, I. M. (1984): Achondrite ALHA77005: Alteration of chromite and olivine. Meteoritics, **19**, 121–133.

STÖFFLER, D., KEIL, K. and SCOTT, E. R. D. (1991): Shock metamorphism of ordinary chondrites. Geochim. Cosmochim. Acta, **55**, 3845–3867.

TREIMAN, A. H. (1985): Amphibole and hercynite spinel in Shergotty and Zagami: Magmatic water, depth of crystallization, and metasomatism. Meteoritics, **20**, 229–243.

TREIMAN, A.H., MCKAY, G.A., BOGGARD, D.D., MITTLEFEHLDT, D.W., WANG, M.S., KELLER, L., LIPSHUTZ, M.E., LINDSTROM, M.M. and GARRISON, D. (1994): Comparison of the LEW88516 and ALHA77005 martian meteorites: Similar but distinct. Meteoritics, **29**, 581–592.

TUTTLE, O.F. and BOWEN, N.L. (1958): Origin of granite in the light of experimental studies in the system $NaAlSi_3O_8$-$KAlSi_3O_8$-SiO_2-H_2O. Geol. Soc. Am. Mem., **74**.

WARREN, P. H. and KALLEMEYN, G. W. (1997): Yamato-793605, EET79001, and other presumed martian meteorites: Compositional clues to their origins. Antarct. Meteorite Res., **10**, 61–81.

(Received March 24, 1997; Revised manuscript accepted June 5, 1997)